

Proposed Method for Simultaneous Inspection of Lift-off and Surface-hardened Depth in Induction-hardened Steel Plate Using Electromagnetic Properties

Tsubasa Yoshinaga,^{1*} Yuji Gotoh,² Shun Onita,³
Takashi Horino,³ and Yoshitaka Misaka³

¹Department of Mechanical and Energy Systems Engineering,
Oita University, 700 Dannoharu, Oita 870-1192, Japan

²Department of Innovative Engineering, Faculty of Science and Technology,
Oita University, 700 Dannoharu, Oita 870-1192, Japan

³Research and Development Headquarters, Neturen Co., Ltd., 141-8639, Japan

(Received November 9, 2021; accepted February 2, 2022)

Keywords: induction-hardened steel, surface-hardened depth, lift-off, 3D nonlinear electromagnetic FEM, electromagnetic nondestructive inspection

The evaluation of surface-hardened depth (D) in induction-hardened steel is important in the guarantee of quality of the steel. If the size of the surface-hardened steel is large, a nondestructive evaluation method is required to inspect the D since destructive testing using, for example, a Vickers hardness tester, becomes difficult. The electromagnetic properties of the hardened layer are different from those of the nonhardened layer in surface-hardened steel. Therefore, it is possible to estimate the D of surface-hardened steel by measuring the difference in these electromagnetic characteristics using an electromagnetic sensor. On the other hand, the detection signal in the electromagnetic sensor is also affected by the distance (lift-off: L_o) between the surface of the hardened steel and the sensor. In this paper, a method for simultaneously measuring the D in a hardened steel plate and L_o is proposed. The usefulness of simultaneous measurement using the proposed inspection method is evaluated by a 3D nonlinear finite element method taking account of the initial B – H (magnetic flux density: B , magnetic field strength: H) curve and the conductivity of the layers with and without hardening in the surface-hardened steel. In addition, an experimental verification is also carried out.

1. Introduction

Because steel can be hardened in a short time, induction-hardened steel is used for axles of large motors, crankshafts of automobiles, railway rails, and large bearing parts of large generators, and so forth. In induction hardening, the depth of the hardened layer is adjusted via the excitation frequency of the induction coil in the induction hardening device. Since the mechanical properties, such as abrasion resistance and fatigue resistance, of the induction-hardened steel change with the surface-hardened depth (D), it is necessary to evaluate the D of

*Corresponding author: e-mail: v20e1049@oita-u.ac.jp
<https://doi.org/10.18494/SAM3703>

the steel. Generally, the D of surface-hardened steel is measured by destructive testing using a Vickers hardness tester,⁽¹⁾ Brinell hardness tester,⁽²⁾ Rockwell hardness tester,⁽³⁾ and so forth. If the size of the surface-hardened steel is large, such destructive testing becomes difficult. Therefore, there is a demand for a nondestructive inspection method that is compact and can evaluate the D without contact. As nondestructive inspection methods for the D , the ultrasonic method,⁽⁴⁾ alternating current potential drop method,⁽⁵⁾ and Barkhausen noise method⁽⁶⁾ have been proposed. Since a contact medium or measurement electrodes are required by the ultrasonic method and the alternating current potential drop method, noncontact inspection is difficult. Barkhausen noise testing requires high detection performance and signal processing technology since the detection signal is weak.

In this paper, we propose a nondestructive inspection method for the D in the surface of an induction-hardened steel plate using only a steady alternating magnetic field and a simple device. The D of the steel plate is measured by detecting the difference in the permeability and conductivity between the hardened and nonhardened layers inside the steel plate using an electromagnetic sensor by an eddy current testing method.^(7–11) On the other hand, in the actual field, it is difficult to maintain the distance (lift-off: L_o) between the surface of the induction-hardened steel and the sensor with high accuracy. This is because the surface of the induction-hardened steel may have a thin nonmetallic coating of unknown thickness such as a rust preventive. Moreover, the thickness of this coating is not uniform. However, the detection signal is also influenced by minute changes in L_o . Therefore, in this research, we propose a method for simultaneously measuring the D in a hardened steel plate and L_o that is not affected by minute fluctuations in L_o .

2. Electromagnetic Properties of Steels with and without Hardening in High-frequency Hardened Steel

In this research, the D is evaluated only for SCM440 steel, which is often used in machine parts. Generally, the maximum D for machine parts is about 5 mm. Therefore, in this paper, the maximum D to be considered is 5.5 mm. This is a chromium molybdenum steel containing 0.38 to 0.43% carbon. Figure 1 shows the hardness distribution inside the induction-hardened SCM440 steel plate as measured by a Vickers hardness tester when the effective surface-hardened depths are 1, 3, and 5.5 mm. In addition, this figure shows the average value of any five locations of each hardened depth steel plate. In this figure, the horizontal axis shows the depth from the surface in the surface-hardened steel plate and the vertical axis shows the Vickers hardness value at the test load of 0.3 kg. In the Japanese Industrial Standards (JIS), the domain where the hardness inside the surface-hardened steel is harder than 400 HV is defined as an effectively hardened layer. This figure shows that in the surface-hardened steel of each D , the maximum hardness (the hardest domain in the surface) is about 650 HV; the hardness of the intermediate layer drops sharply, and the hardness in the nonhardened domain is about 275 HV. Then, the hardened layer of 650 HV and the nonhardened layer of 275 HV in the surface-hardened steel are cut out by electrical discharge machining, and the electromagnetic characteristics of each material are measured.

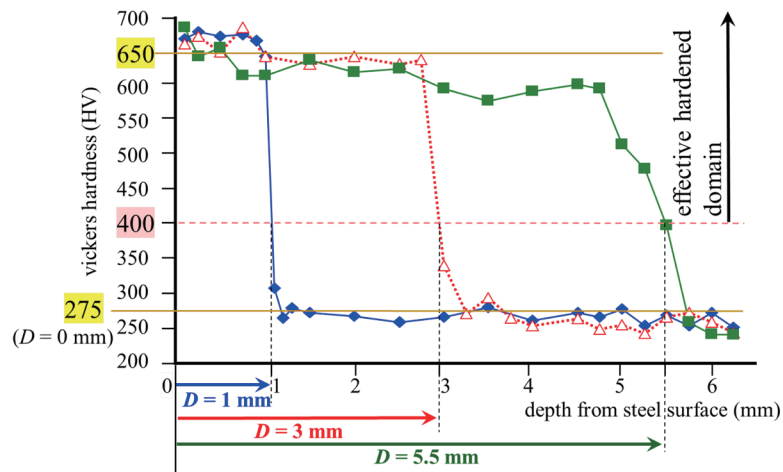


Fig. 1. (Color online) Hardness distribution in surface-hardened steel plate at each depth obtained by Vickers hardness tester (SCM440 steel, Vickers load: 0.3 kgf).

Figure 2 shows the initial magnetization curves of the hardened (650 HV) and nonhardened (275 HV) layers of SCM440 steel. This figure shows that the permeability of the steel is reduced by hardening.⁽¹⁰⁾ The conductivities of the hardened and nonhardened layers in the surface-hardened steel are also measured to be 3.231×10^6 and 3.983×10^6 S/m, respectively. Both the maximum relative permeability and conductivity of the hardened layer are lower than those of the nonhardened layer.

3. Inspection Model and Calculation Method

3.1 Electromagnetic inspection model

Figure 3 shows the inspection model for detecting both the D in the surface-hardened steel plate and the L_o between the electromagnetic sensor and the steel plate. The inspection model is symmetrical about the x -axis regarding the x - y plane, so the model is shown halved. In this paper, a flat plate is used as the induction-hardened steel material for basic research. The proposed electromagnetic sensor consists of an electromagnetic yoke made of laminated silicon steel plate, an alternating excitation coil, and two detection coils. The excitation frequency and current applied to the excitation coil are 10 Hz and 1.5 A (rms), respectively. The flux density (B_z) inside the magnetic yoke is detected with the z -direction detection coil on one leg of the yoke, and the x -direction magnetic field (B_x) distributed between the two legs of the yoke is detected with the x -direction detection coil. These B_x and B_z are evaluated on the basis of the peak values of these waveforms. The surface of induction-hardened steel may be coated with a nonmetallic layer of an unknown thickness such as paint or rust preventive. Therefore, it is difficult to know the exact value of L_o in the actual inspection. In this research, both the L_o and D are estimated using B_x and B_z detected by the two detection coils.

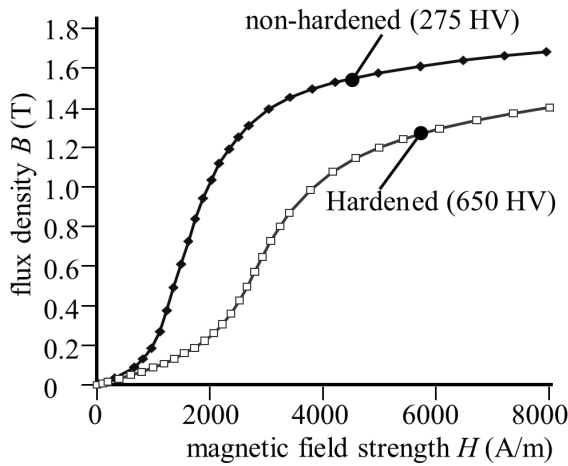


Fig. 2. Initial magnetization curves of the hardened (650 HV) and non-hardened (275 HV) layers of the surface-hardened steel plate (SCM440).

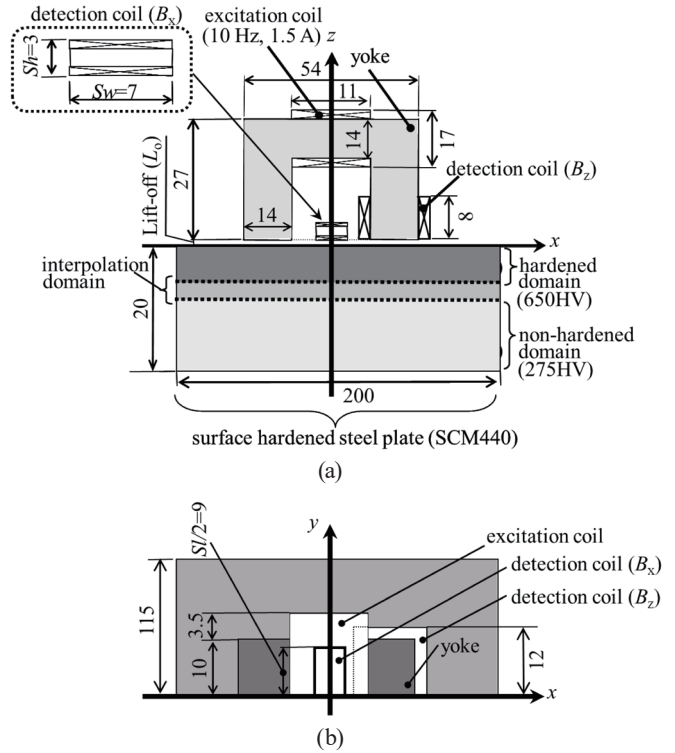


Fig. 3. Proposed inspection electromagnetic sensor and model. (a) $x-z$ plane. (b) $x-y$ plane.

3.2 Method of analysis considering interpolation of magnetization curves and conductivities

In this research, the flux densities (B_x and B_z) in the two detection coils are analyzed by the 3D electromagnetic finite element method (FEM) taking account of the initial magnetization curve and the conductivity of the layers with and without hardening in the surface-hardened steel plate. Since the applied magnetic flux is small for the electromagnetic yoke in this electromagnetic sensor, the relative permeability is calculated at a constant $1000 \times \mu_o$ H/m. Since the magnetic yoke is made of laminated silicon steel sheets, the eddy currents in the magnetic yoke are neglected.

The 3D FEM with first-order hexahedral edge elements are applied. To obtain steady-state results, the computations are performed over three periods (= 96 steps). The time interval Δt of the step-by-step method is chosen as 3.125×10^{-3} s when the excitation frequency is 10 Hz. The basic equations of the electromagnetic field analysis in consideration of the eddy current using the $A-\phi$ method are given by

$$\text{rot}(\nu \text{rot } A) = J_o - \sigma \left(\frac{\partial A}{\partial t} + \text{grad } \phi \right), \tag{1}$$

$$\operatorname{div} \left\{ -\sigma \left(\frac{\partial \mathbf{A}}{\partial t} + \operatorname{grad} \varphi \right) \right\} = 0, \quad (2)$$

where A is the magnetic vector potential, φ is the scalar potential, ν is the reluctivity, J_o is the current density, and σ is the conductivity. The Newton–Raphson (N–R) method is used for the nonlinear iterative calculation of the magnetic characteristic. The N–R iterative calculations are performed using the initial magnetization curve shown in Fig. 2. The conditions for the calculations and measurements are shown in Table 1.

The inside of the surface-hardened steel is divided into a hardened layer, a heat-affected zone, and a nonhardened layer. Therefore, to calculate the flux density inside the hardened steel, a nonlinear electromagnetic field analysis that considers the magnetization curve and the conductivity in these three layers is required. Figure 4 shows an example of the hardness distribution inside the surface-hardened steel plate when the effective hardened depth D is 3

Table 1
Conditions of calculation and measurement.

Excitation coil	Excitation frequency: 10 Hz, Ampere-turns: 1.5 A (rms) \times 60 turns = 90 AT
Search coil (B_x)	x -direction of magnetic field: 175 turns
Search coil (B_z)	z -direction of magnetic field: 95 turns
Lift-off (L_o)	0.1, 0.15, 0.2, 0.25, 0.3 mm
Dimension of specimen	SCM440 steel plate 120 \times 230 \times 20 mm ³
Hardened depth (D)	0, 1, 3, 5 mm
Conductivity	Hardened domain: 3.23×10^6 S/m Non-hardened domain: 3.98×10^6 S/m
Nodes and elements	86436, 78182
Convergence criterion	N–R method: 1.0×10^{-4} T, ICCG method: 1.0×10^{-4}

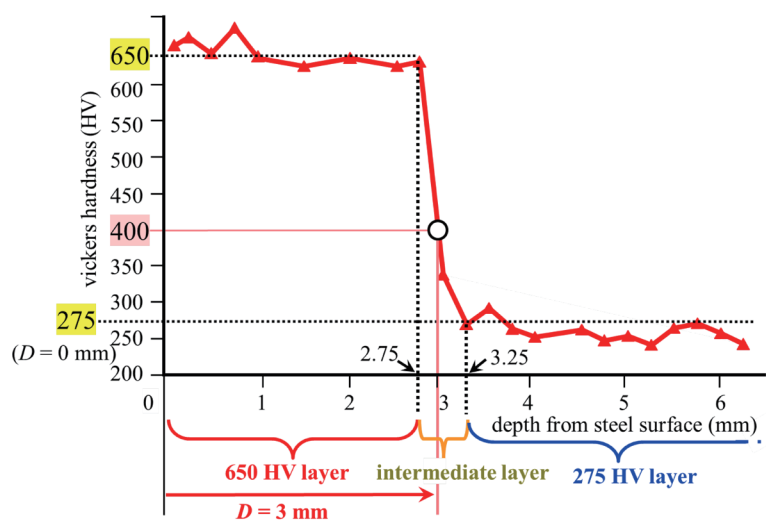


Fig. 4. (Color online) Example of hardness distribution inside surface-hardened steel plate when the effective hardened depth D is 3 mm.

mm. The figure shows that the hardness from the surface in the steel plate to 2.75 mm is about 650 HV. Since the region between the depths of 2.75 and 3.25 mm is the heat-affected zone, the hardness is reduced almost linearly from 650 to 275 HV. The hardness of the region deeper than 3.25 mm is almost constant at about 275 HV. Therefore, in the nonlinear FEM analysis, the initial $B-H$ (magnetic flux density: B , magnetic field strength: H) curve and conductivity of the hardened layer shown in Fig. 2 with a hardness of 650 HV are used for the region from the surface of the hardened steel plate to 2.75 mm, and in the region deeper than 3.25 mm inside the steel plate, the initial $B-H$ curve and conductivity of 275 HV of the nonhardened layer in Fig. 2 are used. On the other hand, the initial $B-H$ curve and conductivity in the heat-affected zone from 2.75 to 3.25 mm depth are obtained by linear interpolation using the magnetization curve and conductivity of the 650 HV hardened layer and the 275 HV nonhardened layer.

3.3 Effects of hardened depth and change in lift-off

The distribution of the flux density inside the steel plate is analyzed when the D and L_o are changed. Figure 5 shows the distribution of the flux density in the steel plate when L_o is constant at 0.1 mm and D is 0 and 5.5 mm. This figure shows that since the permeability and conductivity are lower in the surface-hardened region than in the nonhardened region, the maximum flux density inside the steel plate is decreased when D is increased. Figure 6 shows the effect of D on

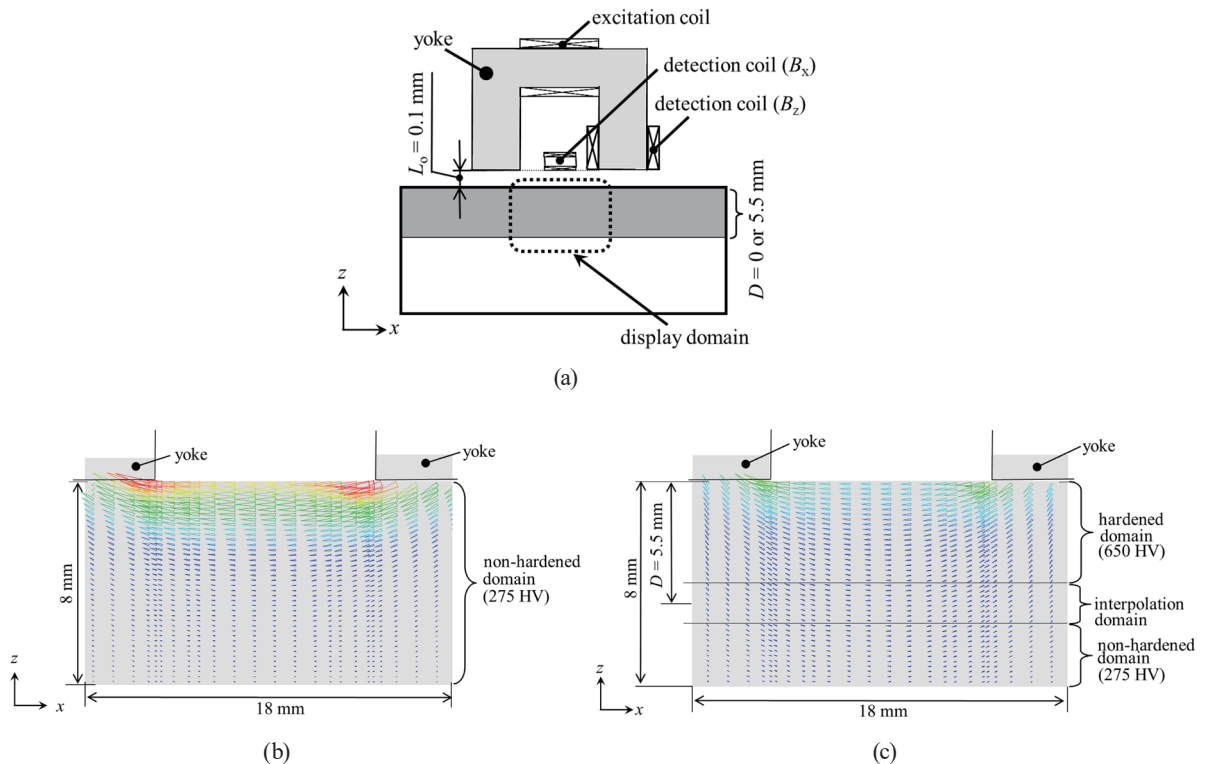


Fig. 5. (Color online) Distribution of the flux density in the steel plate when the surface-hardened depth D is 0 and 5.5 mm ($L_o = 0.1$ mm). (a) Display domain. (b) $D = 0$ mm ($B_{max} = 0.905$ T). (c) $D = 5.5$ mm ($B_{max} = 0.555$ T).

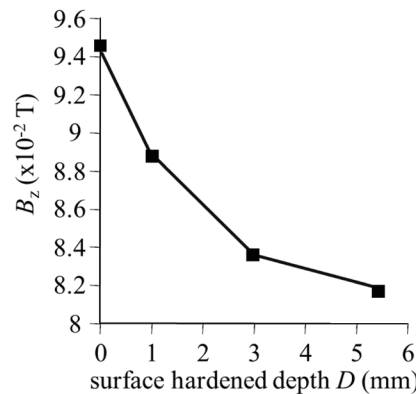


Fig. 6. Effect of surface-hardened depth D on flux density B_z when lift-off L_o is constant at 0.1 mm (calculated).

the calculated flux density B_z in the z -direction detection coil when L_o is constant at 0.1 mm. This figure shows that B_z is decreased when D is increased. This is because the flux density inside the magnetic yoke is decreased when D is increased since the permeability and conductivity are lower inside the surface-hardened layer of the steel plate than in the nonhardened layer. Figure 7 shows the effect of D on the calculated flux density B_x in the x -direction detection coil when L_o is constant at 0.1 mm. This figure shows that B_x is increased when D is increased. This is because the leakage flux distributed in the air between both feet of the yoke is increased since the permeability and conductivity in the surface domain of the steel plate are decreased when D is increased.

Figure 8 shows the distribution of the flux density inside the steel plate when the D is set to 0 mm and the L_o is 0.1 and 0.3 mm. This figure shows that if D is constant, the maximum flux density in the steel plate is decreased when L_o is increased. This is because it becomes difficult for the magnetic flux from the excitation coil to reach the steel plate when L_o is increased. Figure 9 shows the effect of L_o on the calculated flux density B_z in the z -direction detection coil when D is constant at 0 mm. This figure shows that if D is constant, then B_z in the z -direction detection coil is also decreased when L_o is increased, similar to the result in Fig. 6. Therefore, from the results of Figs. 6 and 9, it is difficult to inspect D using only B_z in the z -direction detection coil in the actual field.

Figure 10 shows the effect of the L_o on the calculated flux density B_x in the x -direction detection coil when the D is constant at 0 mm. This figure shows that B_x is increased when L_o is increased, similar to the result in Fig. 7. This is because the impressed magnetic flux from the magnetic yoke is less able to penetrate into the steel plate, and the magnetic flux distributed between the two legs of the yoke is increased. Therefore, from the results of Figs. 7 and 10, it is difficult to inspect D using only B_x in the x -direction detection coil in the actual field. However, from the above results, the changes in B_x and B_z are different when only D is changed and when only L_o is changed. Therefore, a method for estimating both D and L_o is considered using the results for both B_x and B_z .

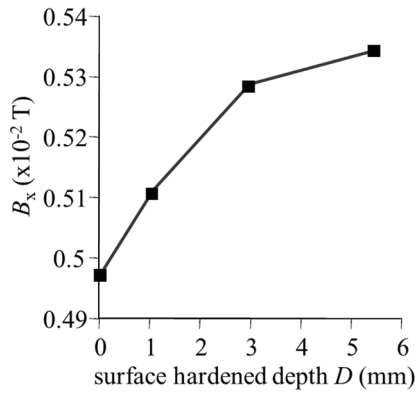


Fig. 7. Effect of surface-hardened depth D on flux density B_x when lift-off L_o is constant at 0.1 mm (calculated).

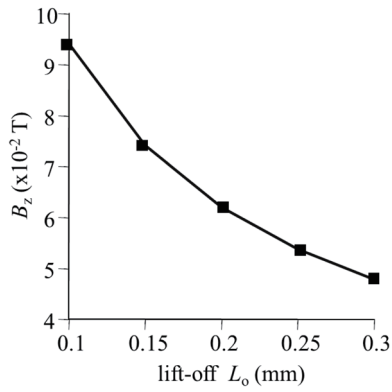


Fig. 9. Effect of lift-off L_o on flux density B_z when surface-hardened depth D is constant at 0 mm (calculated).

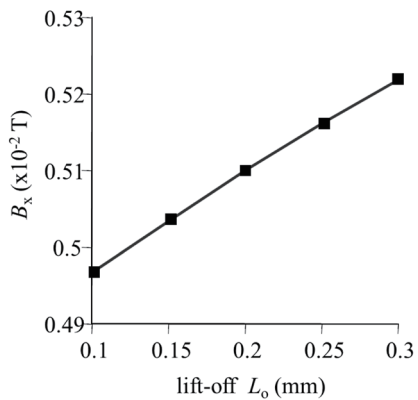
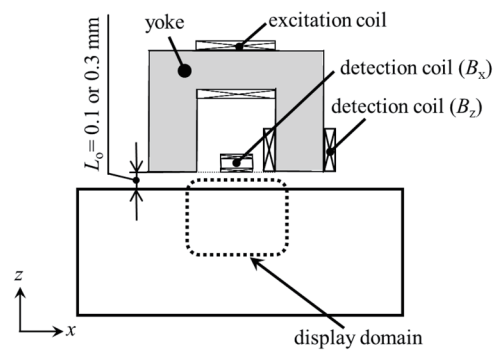
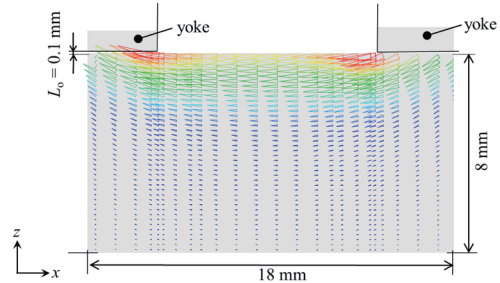


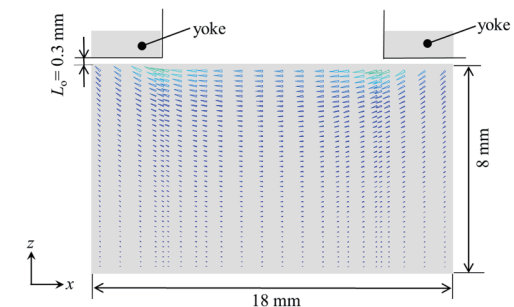
Fig. 10. Effect of lift-off L_o on flux density B_x when surface-hardened depth D is constant at 0 mm (calculated).



(a)



(b)



(c)

Fig. 8. (Color online) Distribution of flux density inside steel plate when lift-off L_o is 0.1 and 0.3 mm ($D = 0$ mm). (a) Display domain. (b) $L_o = 0.1$ mm ($B_{max} = 0.905$ T). (c) $L_o = 0.3$ mm ($B_{max} = 0.323$ T).

4. Method of Measuring Both Surface-hardened Depth and Lift-off

The x -direction flux density B_x and z -direction flux density B_z obtained in each detection coil are measured when D in the surface-hardened steel plate is changed for each L_o . Figure 11 shows the measured B_x and B_z in the x - and z -direction detection coils obtained by changing D and L_o . In this figure, B_x is shown on the vertical axis and B_z is shown on the horizontal axis. This figure shows that if L_o is constant, then B_x is increased and B_z is decreased when D is increased. The changes in B_x and B_z with D showed a similar trend to the results of the 3D FEM. On the other hand, if D is constant, then B_x is increased and B_z is decreased when L_o is increased. This is because B_z in the closed magnetic path between the magnetic yoke and the steel plate is reduced when L_o is increased, and B_x distributed between both legs of the yoke is increased.

The figure shows that the changes in the signals of B_x and B_z due to the changes in D and L_o can be distinguished in this model. In this research, the unknown D and L_o are both evaluated by linear interpolation using the values in Fig. 11 with the measured B_x and B_z in the two detection coils. Table 2 shows the results of D and L_o obtained by interpolation using the B_x - B_z plane of Fig. 11. For the "measured hardened depth" values in Table 2, the measurement results of the specimens as shown in Fig. 1 are shown. The measured values are almost in agreement with the obtained ones. The table illustrates that both D and L_o can be detected from B_x and B_z in the two detection coils in this model.

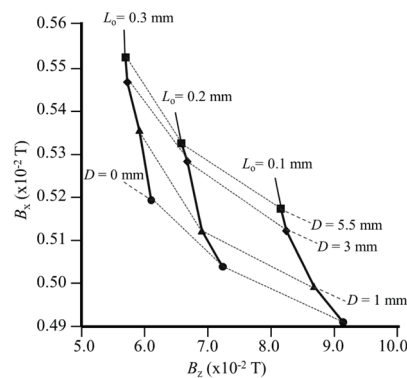


Fig. 11. B_x and B_z in the x - and z -direction detection coils obtained by changing surface-hardened depth D and lift-off L_o (measured).

Table 2
Conditions of calculation and measurement.

Factors	Measured	Interpolated	Error (mm)
Depth D (mm)	1	0.92	0.08
Lift-off L_o (mm)	0.15	0.133	0.017
Depth D (mm)	3	2.62	0.38
Lift-off L_o (mm)	0.15	0.185	0.035
Depth D (mm)	3	2.88	0.12
Lift-off L_o (mm)	0.25	0.184	0.066
Depth D (mm)	5.5	5.35	0.15
Lift-off L_o (mm)	0.25	0.177	0.073

5. Conclusions

The results obtained are summarized as follows:

- (1) It is possible to estimate the hardened depth D of a surface-hardened steel plate by detecting the change in flux density due to the differences in the permeability and conductivity in the steel with and without hardened layers. However, the flux density detected by each detection coil is influenced by the changes in both the lift-off L_o and depth D of the surface-hardened steel.
- (2) The flux density B_x in the x -direction detection coil is increased and the flux density B_z in the z -direction detection coil is decreased when D or L_o of the induction-hardened steel is increased. However, the changes in the signals of B_x and B_z in the two detection coils due to the changes in D and L_o can be distinguished. Therefore, it is possible to inspect both D and L_o by detecting both B_x and B_z of the two detection coils in the proposed inspection sensor.

The elucidation of details of the physical phenomena leading to changes in the permeability and conductivity of the hardened steel due to induction hardening and the effects of material and shape changes on induction-hardened steel in the proposed inspection method are future research subjects. The evaluation of different materials or hardened depths deeper than 5 mm in this inspection method is a future research subject.

References

- 1 T. Sugimoto and T. Kawaguchi: IEEE Trans. Ind. Electron. **44** (1997) 696. <https://doi.org/10.1109/41.633474>
- 2 O. Richmond, H. L. Morrison, and M. L. Devenpeck: Int. J. Mech. Sci. **16** (1974) 75. [https://doi.org/10.1016/0020-7403\(74\)90034-4](https://doi.org/10.1016/0020-7403(74)90034-4)
- 3 H. Zhang, H. Fu, Y. Jiang, H. Guo, Y. Lei, R. Zhou, and Q. Cen: Mater. Sci. Eng. Technol. **42** (2011) 765. <https://doi.org/10.1002/mawe.201100753>
- 4 A. H. Hamzehkanloo: J. Sci. Tech. **13** (2021) 49. <https://doi.org/10.5958/2349-2988.2021.00009.7>
- 5 J. Zhang, S. Xie, X. Wang, Y. Li., and Z. Chen: IEEE Trans. Magn. **48** (2012) 375. <https://doi.org/10.1109/TMAG.2011.2172679>
- 6 F. A. Franco, M. F. R. Gonzalez, M. F. de Campos, and L. R. Padovese: J. Nondestruct. Eval. **32** (2013) 93. <https://doi.org/10.1007/s10921-012-0162-8>
- 7 J. Marcus, L. Chester, H. Scott, and K. Emily: Electromagnetic Nondestructive Evaluation (IX) (2005) 135. <https://www.researchgate.net/publication/268354528>
- 8 Y. Kai, Y. Tsuchida, and M. Enokizono: J. Optoelectron. Adv. Mater. **10** (2008) 1078. <https://www.researchgate.net/publication/290555035>
- 9 Y. Gotoh, N. Sasaguri, and N. Takahashi: IEEE Trans. Magn. **46** (2010) 3137. <https://doi.org/10.1109/TMAG.2010.2043232>
- 10 Y. Gotoh, S. Onita, T. Horino, and Y. Mikasa: IEEE Trans. Magn. **54** (2018) Article Sequence Number:6202404. <https://doi.org/10.1109/INTMAG.2018.8508724>
- 11 Y. Kai: Electromagnetic Nondestructive Evaluation (VIII) (2004) 153.